Proceedings of ASME 2012 11th Biennnial Conference on Engineering Systems Design and Analysis
ESDA 2012
July 2-4, 2012, Nantes, France

ESDA2012-82332

DRAFT: EXPERIMENTAL STUDY OF VERY LOW ASPECT RATIO WINGS IN SLENDER BODIES

M.A. Arevalo-Campillos

E. T. S. Ingenieros Industriales
Universidad de Málaga
Dr Ortiz Ramos s/n
29071 Málaga
Spain

S. Tuling*

Council for Scientific and Industrial Research
P.O. Box 395
Pretoria
0001
South Africa
stuling@csir.co.za

L. Parras

E. T. S. Ingenieros Industriales
Universidad de Málaga
Dr Ortiz Ramos s/n
29071 Málaga
Spain

C. del Pino

E. T. S. Ingenieros Industriales
Universidad de Málaga
Dr Ortiz Ramos s/n
29071 Málaga
Spain

L. Dala

University of the Witwatersrand
1 Jan Smuts Avenue
Johannesburg
2050
South Africa

ABSTRACT

The dynamics of very low aspect ratio wings (or strakes) vortices in slender bodies are complex due to the interaction of the shed vortex sheet and the body vortex. For missiles at supersonic speeds these interactions are not easily predicted using engineering level tools. To shed some new light onto this problem, an experimental study in a water channel for moderate Reynolds number (Re=1000) was performed for a 19D body and strake configuration with strakes having a span to body diameter ratio of 1.25. Comparisons to numerical simulations in supersonic flow are also performed. Flow visualisation has been carried out to characterize the vortex dynamics at different angles of attack; these being 11°, 16°, 22°and 27°. The comparison between a slender body without strakes and the body-strake configuration has given some key indicators in relation to the vortex position of the core. Furthermore, unsteady wing-body interference has been observed at angles of attack above 20°for both experimental and numerical simulations. Consequently, the average position of the vortex core is located at larger distances from the missile in comparison to the body without strakes. The numerical simulations show good correlation with the experimental tests even though the dynamic convective interactions between the body vortex and strake vortex sheet are not predicted.

NOMENCLATURE

A_{TS} Area of the tunnel test section
D Body diameter
K_{B_W} Wing-to-body carryover factor
Re Reynolds number
T Temperature
V Body velocity

*Address all correspondence to this author.

(x,y,z) Experimental Coordinate System (ECS)
(x',y',z') Body Coordinate System (BCS)
z Non-dimensional axial distance (z/D)
z_M Non-dimensional axial distances at which the wing-body vortices merge
α Angle of Attack
ν Kinematic viscosity

INTRODUCTION

The interaction between wings and bodies for slender body configurations has been the subject of numerous studies in the past [1] [2]. Potential methods have in the past, and still remain the only theoretical methods for determining these interactions. At an engineering prediction level the theoretical methods suffice for wings of low to moderate aspect ratio. For wing body combinations with very low aspect ratio wings having side edges which are a significant length of the configuration, the overall body loads are not reasonably predicted. Current methods accounting for these effects are based on experimental databases [3] [2], and unfortunately, the limitations of the experimental configurations. Studies in the past [4] [5] have only peripherally touched on the aerodynamic phenomena causing this discrepancy between the original formulations based on slender body theory and the observed loads. One of the traditional methods for predicting gross loads of a body and wing combination is to algebraically sum the individual components i.e. body and wing, and their interactions i.e. wing-to-body and body-to-wing. At the gross loads level, the wing-to-body carryover factor, K_{B_W}, is poorly predicted [4] [5]. A previous numerical study by Tuling and Dala [5] on these interactions has indicated possible complex vortex interactions of the body with very low aspect ratio wings or strakes. The configuration of the strakes are dominated by its side edge that makes the strake a rectangular wing for all intensive purposes except for the leading.

To this end, experimental studies of the flow phenomena and their dynamics is intended to shed some light on the possible reason for the observed discrepancies. In addition to this fewer studies are concerned about the three dimensional velocity field measurements of vortex dynamics [6] or flow visualisation [7] for such configurations. Expected flow regimes as a function of angle of attack are symmetric, unsteady, or non-symmetric and unsteady.

For slender body wing combinations, the dominant speed regime of application is transonic to supersonic, as reflected in by the work performed by Tuling and Dala. The experimental study executed in this paper was performed at low speed because the slender body assumption where the changes in the dominant flow direction are small compared to other two dimensions are applicable.

The geometry used in this work is the same as that used by Tuling and Dala [5], which is a 19D tangent-ogive body with cruciform 11.25D strakes with a span to body diameter ration of 1.25. The nose and aft body are 3D in length, whilst the strakes had a 45°leading edge sweep. The strakes are tested in the '+' configuration. For the configuration of reference [5] the diameter of 80mm was used. For the experimental study a body diameter of 16mm was used.

NUMERICAL SIMULATIONS

For comparison purposes and because this work follows on from the numerical studies of reference [5], additional numerical simulations were performed to match the experimental conditions of this study. In summary, the numerical simulations were performed using Fluent with the Spalart-Allmaras turbulence model with near wall treatment. These simulations were performed at the supersonic speeds of Mach 2.0, 2.5 and 3.0. Little difference between the flow structures between Mach 2.0, 2.5 and 3.0 were observed, and all the comparisons presented are for the Mach number 2.0. The vortex positions of shed vortices of the numerical simulations (for comparison to the experimental tests) were determined by extracting the local minimum of the $\lambda_2 - criterion$ [8] at any plane of interest perpendicular to the body axes of the configuration.

EXPERIMENTAL SETUP AND TEST CONDITIONS

The experiments were carried out in a water towing tank with a working section of 0.5m x 0.5m and 5m long installed at the Laboratory of Aero-Hydrodynamics of Vehicles at the University of Málaga. The test section is made of Plexiglas to allow for optical visualisation. A sketch of the experimental set up is depicted in 1.

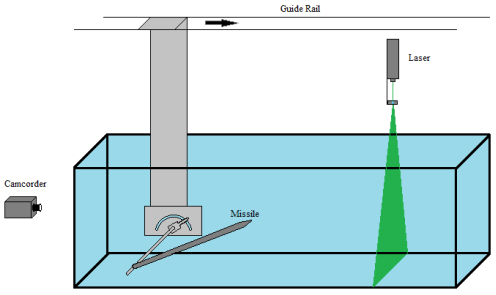

FIGURE 1. EXPERIMENTAL SETUP OVERVIEW

The missile is attached to a specially manufactured device

that allows the angle of attack to be changed. This detail is presented in 2, where both the anchor devices and the missile are shown. The body moves through the towing tank by means of a controlled linear guide rail and is driven by a DC motor with an encoder and controlled by a PC.

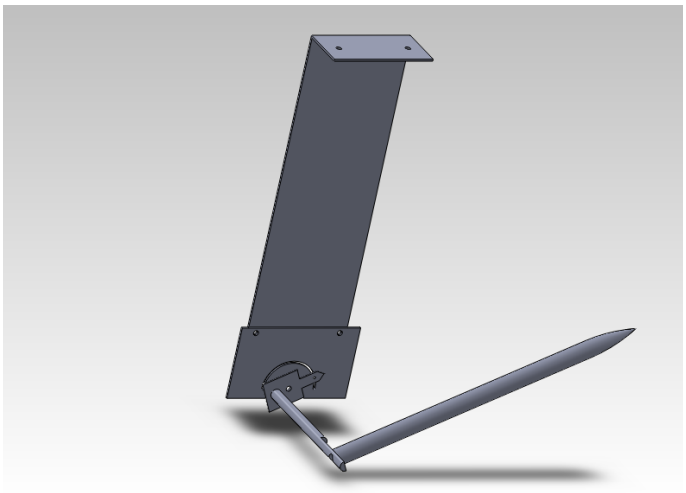

FIGURE 2. MISSILE WITHOUT STRAKES AND MOUNTING SYSTEM

The values of the angle of attack are typically the ones used in missile aerodynamics (from 5 to 30 degrees). A set of five different angles of attack where used (6.5°±0.3, 11°±0.3, 16°±0.2, 22°±0.05 and 27°±0.05). The velocity imposed to the missile is about 57 mm/s ±1 mm/s. The water temperature is measured with a PT100 probe to within ±0.1 °C. The Reynolds number is defined as $Re = VD/\nu$ and reaches a constant value of 1040 ±3 . Special care was taken to obtain a steady state regime with no velocity fluctuations. The missile was thus smoothly accelerated until it reached a constant velocity and the results were checked to ensure that they were not dependent on the acceleration. The two configurations of body alone and body plus strakes were tested in an attempt to understand the change in leeside vortex behaviour and compare the results to the numerical simulations.

Flow visualisation was carried out using a green fluorescent dye (Rhodamine 6G) mixed with a retardant gel. The dye was applied on the forebody zone. This area was found to better highlight the fluid dynamics. The test area was illuminated normally to the mean flow with a laser sheet from a green laser of 500mW (wavelength = 532nm). A set of lens and optics were used to create a thin laser sheet.

A 1Mpixel video-camera was used to capture the vortex images at a frame rate of 1/25s. The frame rate was found to be well suited to have enough accuracy in the axial resolution of the flow structures which can be resolved to an axial step below 0.15D. The processed images were extracted from a video and then post-processed to quantify the vortex core position from both the body and the strakes.

FLOW VISUALISATION

The comparison of different frames between the missile with and without strakes is presented in this section. First, we will discuss the different coordinate systems used in this study to compare the results with those presented in [5].

Experimental and Body Coordinate Systems

Due to the experimental setup, flow visualisations were performed in a x-y plane, which corresponds to an experimental coordinate system (ECS). The origin of this system being the rocket nose. The results were converted to the body coordinate system (BCS); this being a more common axes system for missile aerodynamics. This is shown in 3.

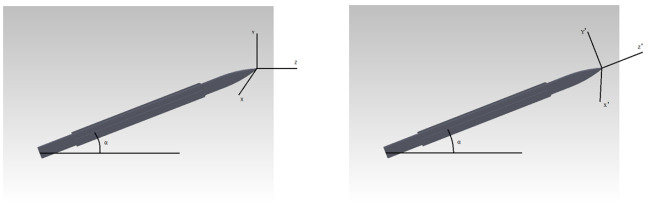

(a) (b)

FIGURE 3. EXPERIMENTAL (a) AND BODY (b) COORDINATE SYSTEMS FOR A CONSTANT ANGLE OF ATTACK

The transformations used are as follows:

$$x' = x \tag{1}$$

$$y' = (y - z\tan(\alpha))\cos(\alpha) \tag{2}$$

$$z' = \frac{z}{\cos(\alpha)} - \frac{2y'}{\sin(2\alpha)} \tag{3}$$

The BCS is identified by the primes.

Flow Visualisation

Figure 4 shows representative pictures of the body and body plus strake configurations in the non-dimensional length $z' = z/[D\cos(\alpha)]$, where D is the diameter of the body, from the tip of the body.

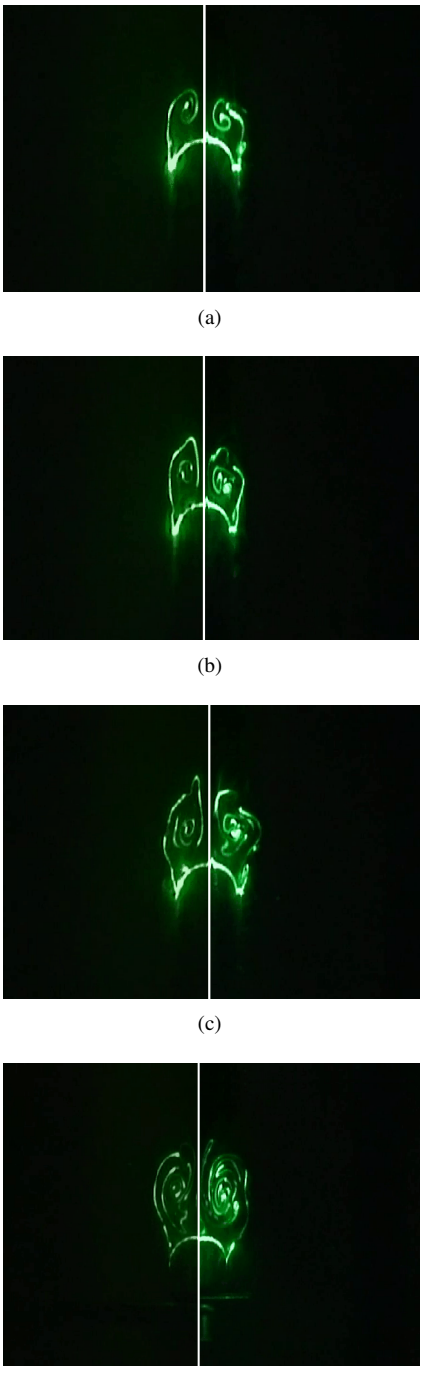

(a)

(b)

(c)

(d)

FIGURE 4. FLOW PATTERNS OF THE BODY (LEFT) AND BODY-STRAKE (RIGHT) AT 27°FOR THE NON)DIMENSIONAL AXIAL DISTANCES OF z'= 7 (a), 9.4 (b), 12.6 (c) and 16.4 (d)

For the body alone configuration (left hand side of the figures), the development of the vortex body is clearly shown in these images. The main vortex starts at the nose due to the non zero angle of attack, and as the flow develops along the body axial length its intensity and characteristic radius increases. For the body and strake configuration (right hand side), a different behaviour is observed. The strake side edge vortex, once starting upstream, approaches the body vortex (see, Figure 4 (a)). Moving downstream (z'=9.4, Figure 4 (b)) a second vortex emanates from the strake and the body-wing interference is clearly observed. However, one can distinguish both structures, since they do not merge. Moving further downstream, (z'=12.6, Figure 4 (c)) the strake and the body vortices are clearly interacting with each other. Further downstream, additional vortices from the strake start. At the end of strakes or towards the end of configuration (z'=16.4, Figure 4 (d)), the vortices have merged into a single vortex.

It should be noted that for all the angles of attack under consideration except at 6.5°, a symmetric body vortex is shed for the body and strake configuration. This is shown in Figure 5 for the angles of attack of 11°, 16°, 22°and 27°at z'=4.75D.

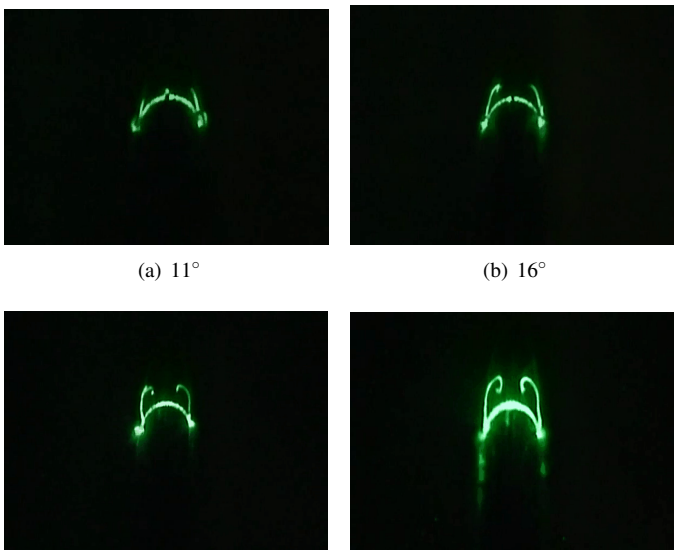

(a) 11°

(b) 16°

(c) 22°

(d) 27°

FIGURE 5. BODY VORTEX FOR VARIOUS ANGLES OF ATTACK AT 4.75D in ECS

Finally, it is worth mentioning that the presence of strake vortices were not observed at angles of attack lower or equal than 6.5°.

POST PROCESSED IMAGES

Firstly, to quantify the flow visualisations, the position of the center of mass is determined as illustrated in Figure 6 for

an angle of attack of 27°at the axial station 5.7D. The blue and red points are the centroid of the strake and body vortices, respectively. To compute these positions post-processing of the video extracted images extracted was performed. A specific analysis was conducted performing image-processing routines to enhance and segment each frame. A geometric analysis would typically be carried out for the segmented image. Looking at the thresholded-segmented image or edge segmented image one would be able to compute the centroid property and to provide this as a coordinate in space (for more details, see reference [7]). The calibration from pixel to real dimensions is done taking the body diameter in the x-axis. Turning our attention to the complete missile with strakes, which is in contrast to figures 3 and 4 which showed a composition built by the half-missile configuration with or without strakes. In addition, it should be emphasized that the flow is symmetric for the body and strake configuration at the axial location before the start of the strakes. Similar observations were observed in the body only configuration (though not shown) for all the angles of attack studied.

FIGURE 6. STRAKES (BLUE DOTS) AND BODY (RED DOTS) VORTEX CORES AT 27°AT 5.7D

The symmetry of the flow is almost guaranteed all over the configuration. The start of asymmetric flow is related to the body-wing interference. As an example, we plot in figure 7 the three dimensional composition of the flow visualisation for 27°. Isocontours of the light intensity are depicted in this figure to highlight the structure of the flow.

Another result that can be easily shown is the three dimensional evolution of the vortex core positions of both the body and the strake vortices. This is shown in figure 8, where the positions (x',y',z') are presented in the body coordinate system. The strake vortices at high angles of attack appear continuous and unbroken. Figure 8 illustrates the interaction between the body and strake vortices, which are identified by the blue and red dots respectively. It can be seen that the vortex interaction increases with

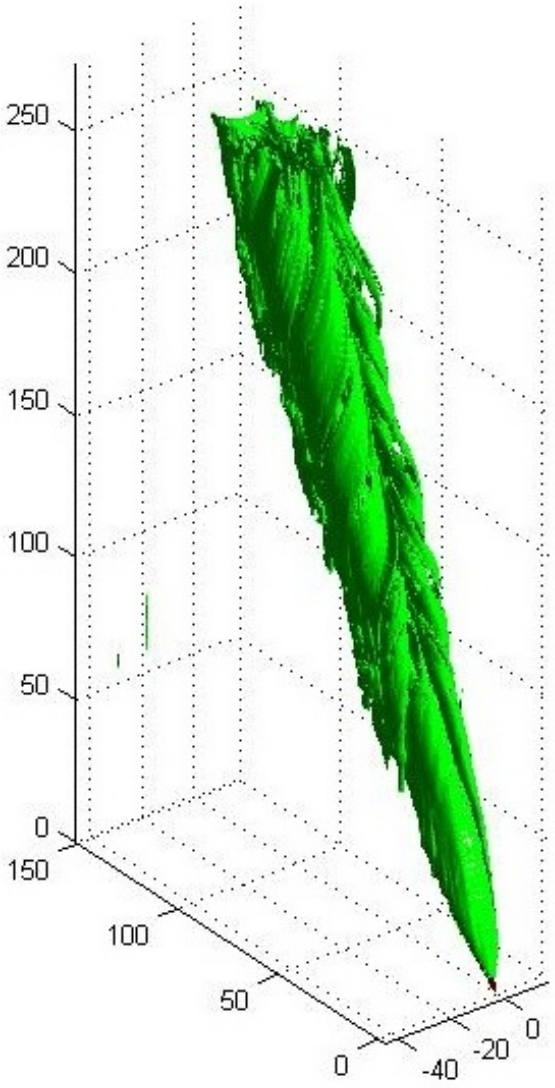

FIGURE 7. THREE DIMENSIONAL PICTURE BUILT FROM THE LIGHT INTENSITY FOR EACH FRAME AT 27°

increasing the angle of attack, or alternatively put, the vortices interact closer to the nose of the body even though the body vortex is at a higher vertical location at higher angles of attack. The interaction is small for 11°, 16°and 22°, and it can be seen that vortices merge after one to three cycles of interaction. This is not the case for the angle of attack of 27°, where the two vortices do not merge into one till they reach almost the missile tail. Thus, it has been shown in these three dimensional views that one can analyze the axial evolution of the vortex core positions and, consequently, it is possible to determine the distances from the tip of missile from where the vortices merge with one another. As it is

shown in Figure 9 (a), we can project the positions of the vortex core shown in Figure 8(d) in a (x',z')-plane. One can observe again in Figure 9(a) that though the positions of vortex cores of both the strake and the body are equal for a certain instant of time (or z'), the vortices do not merge till a critical axial distance. This distance is defined as when the differences in the x'(z') function are less than 0.02 non-dimensional distances. The critical axial position of z' where the two vortices joined together, z_M, as a function of α is shown in Figure 9(b). For the angles of attack considered in this experimental work, it is observed a linear dependency exists. The equation that described this relationship for the experimental data is $z_M = 0.41\alpha + 5.32$.

To better appreciate the difference between the body and the experimental coordinate systems presented above, we plot the centroid coordinates non-dimensionalised with the body diameter. As it is shown in Figure 10(a), we can project the positions of the vortex core in the original (x,y)-plane. Thus, the only information that can be obtained in a local system is the interaction between the vortices and how the centroid moves in any direction. As mentioned above, the flow is symmetric before the body-strake interference starts. In the body coordinate system once the vortices merge, the position in the x'-axis is almost constant, as in the y'-axis the evolution of the vortex is related to the downstream movement and the interaction (symmetry break-up) of both the body and strake vortices. In addition, we can define an average position of the vortex cores. This is shown with a green point in Figure 10(b).

Computing the average position of the vortices, it is useful to know how this parameter depends on the angle of attack. Special attention is given to the values in the y'-axis, as it is the most representative parameter. This is shown in Figure 11, where the average position of y' is plotted against the angle of attack for both missiles (with and without strakes in red and blue lines, respectively). Error bars are estimated with the standard deviation of the mean average position. One can distinguish how the missile without strakes has a smooth increment of the average, since the body with strakes has a sudden increment of its position for an critical angle of attack close to 20.

A reasonable explanation of this fact is found in the non-steady behaviour found in the body-wing interference at angles of attack close to 22°. For a certain critical angle of attack, the strake vortices start to shed continuous, and consequently generate vorticity in an area close to the strake. The body vortices, once they reach the axial station of the start of the strakes become free vortices and start to travel at the local freestream velocity. This results in the body vortices travelling faster away from the body and subsequently merging with the strake vortex. Consequently, the average vortex position is larger than in the case of no strakes.

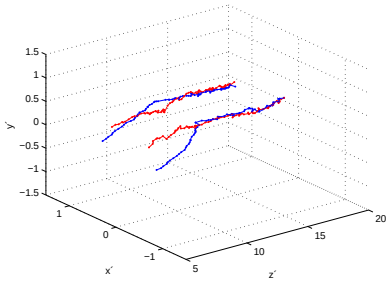

(a) 11°

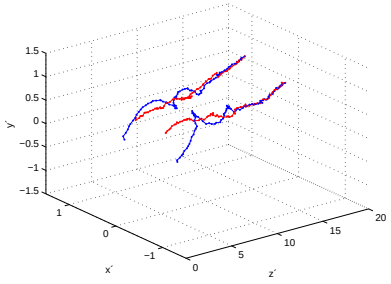

(b) 16°

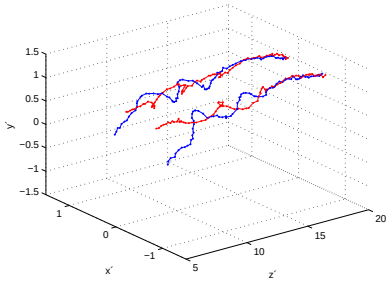

(c) 22°

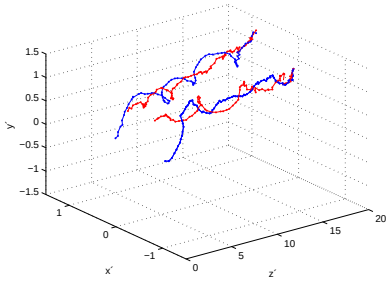

(d) 27°

FIGURE 8. THREE DIMENSIONAL PATHS OF THE VORTEX CORES FOR 11°(a), 16°(b), 22°(c) and 27°(d)

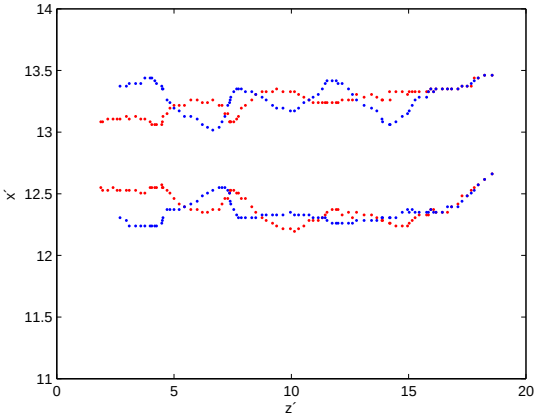

(a)

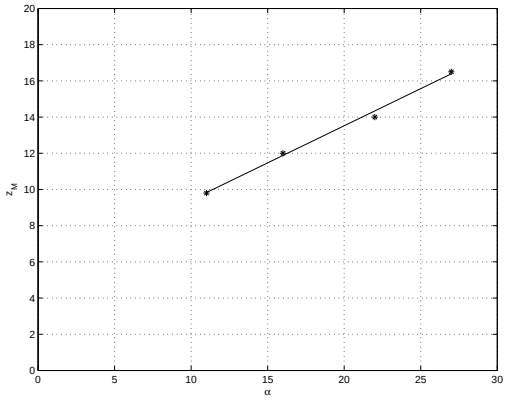

(b)

FIGURE 9. x'-z' PLANE PROJECTION AT 27°AND THE NON-DIMENSIONAL AXIAL POSITION WHERE VORTICES MERGE

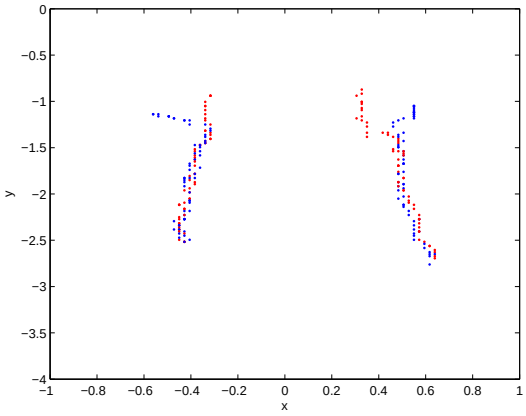

(a) ECS

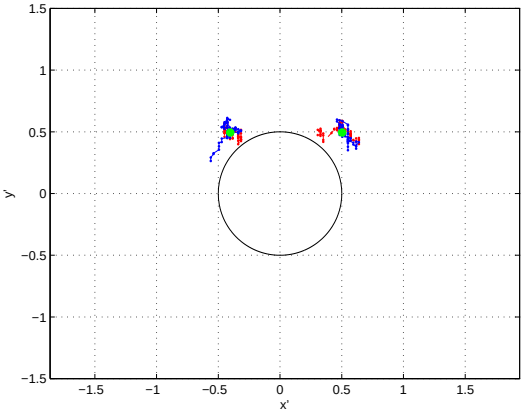

(b) BCS

FIGURE 10. COMPARISON OF ECS (a) AND BCS (b) POSITIONS OF THE VORTEX CORES FOR THE BODY VORTEX (RED) AND STRAKE VORTEX (BLUE) AT 11° (AVERAGE POSITION IN GREEN)

NUMERICAL AND EXPERIMENTAL COMPARISONS

A comparison between the experimental and the numerical results are shown in Figure 12. The experiment represents the flow for an incompressible viscous fluid and the numerics represent the viscous compressible solution. As mentioned previously, the slender body assumption of changes in the axial direction being insignificant and thus an incompressible simulation being applicable for the high speed case is borne out in the experimental observations. Even though the observed flow is in the experimental coordinate system and the numerical simulations are in body coordinate system one can observe the similarities in both structures at an angle of attack of 27 degrees and for the same distance of z'=5.7D from the nose of the missile. As mentioned previously the numerical simulations identify the vortices using the $\lambda_2 - criterion$ and identify two distinct vortices being shed from the body, whilst the experimental tests indicate the body vortex sheet rolling into a single, though elongated, vortex.

Even though the flow structures are similar, the numerical simulations for supersonic flows do, however, reveal differences to that of the incompressible experimental tests. Before these differences are discussed, it should be noted that the secondary vortex shed in the junction of the strake and body in the lee side of the flow is not identifiable by the experimental tests because the dye was applied to the underside of the nose of the body whilst the laser sheet illuminated the upper part of the body (see Figure 1).

The first difference is the shedding of the body vortex whose development is illustrated in Figure 13. As for the experimental tests, no body vortex is present at 6.5°at the axial location where the strakes start i.e. z'=4.75D. For the angles of attack of 11°and

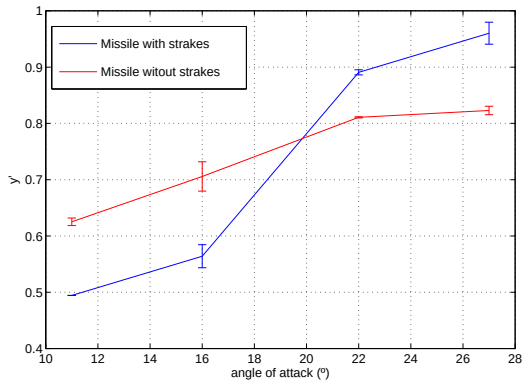

FIGURE 11. THE y' COORDINATE AS A FUNCTION OF ANGLE OF ATTACK

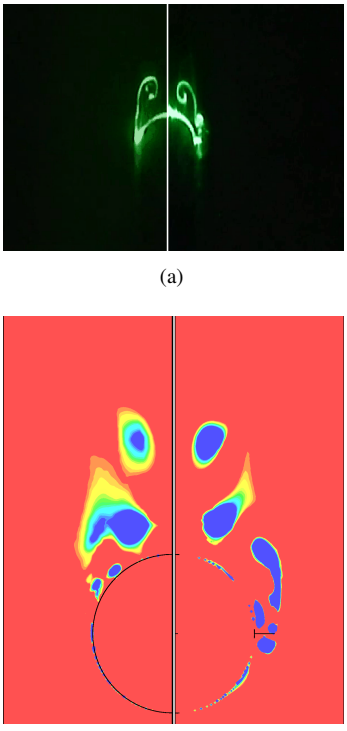

(a)

(b)

FIGURE 12. COMPARISON OF EXPERIMENTAL AND NUMERICAL SIMULATIONS

16°, the body vortex is less well developed in the numerical simulations than for the experimental tests. For and angle of attack of 11°, the body vortex does not interact with the strake vortex due to its low strength and its proximity from the strake vortex. It should be noted that the vortex centroids are determined using the $\lambda_2 - criterion$.

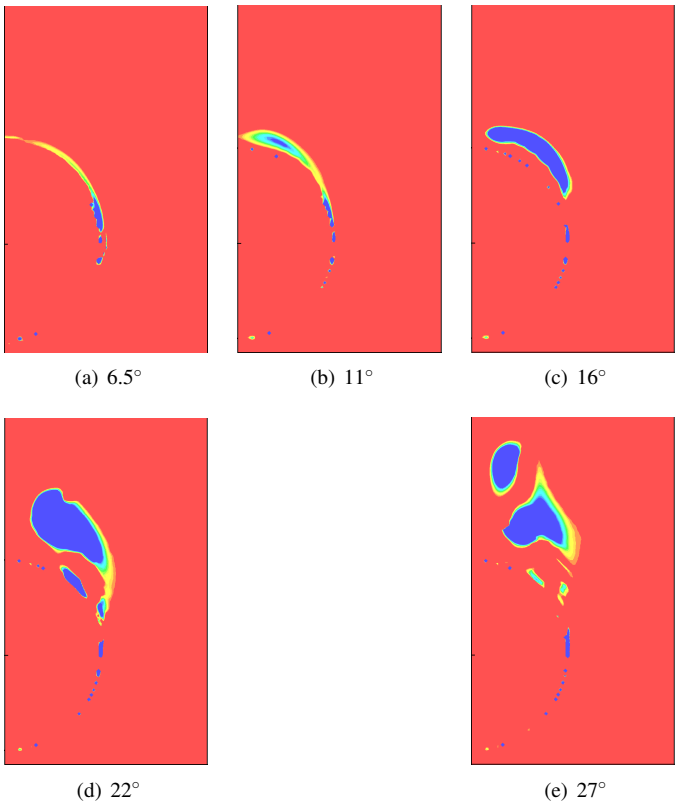

(a) 6.5° (b) 11° (c) 16°

(d) 22° (e) 27°

FIGURE 13. NUMERICAL SIMULATIONS OF BODY VORTEX AT 4.75D

The second difference between experimental and numerical simulations is the interaction of the body vortex and strake vortex sheet. Two distinct types of flow are predicted by the numerical simulations. At moderate angles (11°and 16°) the lees side flow is dominated by the strake vortex sheet which rolls up into a single concentrated vortex. This is illustrated in Figure 14. Above 20°the flow is unsteady in nature, this being similar to the experimental tests. In this regime, the side edge vortex sheet is not shed as a single continuous sheet but rather as multiple sheets. This is illustrated in Figure 15 for the angle of attack of 22°. For the angle of attack of 27°the lee side flow is similar.

At 16°angle of attack the body vortex merges with the strake vortex at an axial station of approximately 8D. This differs considerably with the incompressible experimental tests where the merge occurs at 12D. As can be seen in Figure 16, the secondary separation vortex in the strake body junction is predicted.

For both the angles of attack of 22°and 27°, the body vortex merges with the first part of the strake vortex sheet at 7.5D

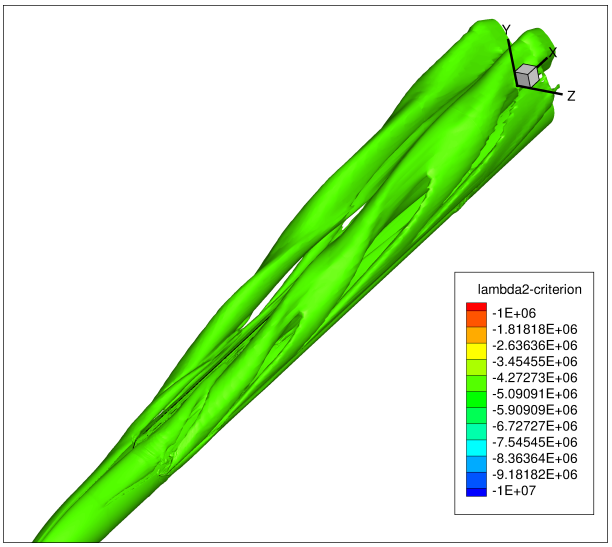

FIGURE 14. NUMERICAL SIMULATIONS OF BODY AND STRAKE VORTEX DEVELOPMENT AT 16°

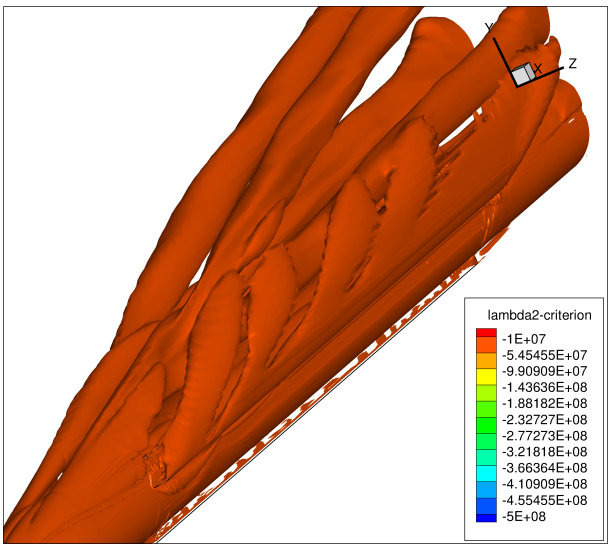

FIGURE 15. NUMERICAL SIMULATIONS OF BODY AND STRAKE VORTEX DEVELOPMENT AT 22°

whilst the bottom core merges with the subsequent strake vortex sheet and travels along the body at approximately the same location. One of the differences in character of the body vortex and strake vortex sheet interaction is that the numerical simulations do not predict the convective stage of interaction between the body vortex and strake vortex sheet (see Figures 4 and 15). This probably manifests itself in the observed differences as to where they merge. The vortex position with axial distance for

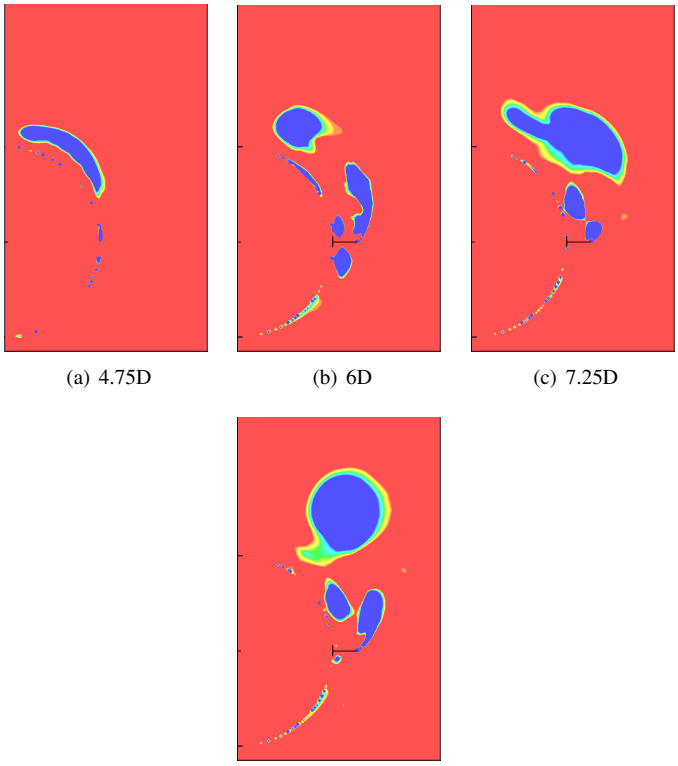

(a) 4.75D (b) 6D (c) 7.25D

(d) 8.5D

FIGURE 16. NUMERICAL SIMULATIONS OF BODY AND STRAKE VORTEX DEVELOPMENT AT 16°

the four angles of attack of interest are compared in Figure 17. It should be noted that the vortex positions were not calculated for many points because of the less dynamic nature of vortex movement. For the 22°and 27°angles of attack, the numerical simulation vortex path compares reasonably well with the experimental results. For the angle of attack of 16°, only the initial locations don't compare well, whereas for the angle of attack of 11°the numerical simulations predict that the merged body and strake vortex travels further away from the body as the axial distance increases.

CONCLUSIONS

Flow visualisation has been performed to characterize the vortex dynamics at different angles of attack for a missile with and without strakes with a particular view to validating and comparing against numerical simulations. The presence of strake vortices were not observed at angles of attack lower than 6.5°, thus confirming that at very small angles of attack the strakes do not affect the vortex body dynamics. At higher angles of attack, the growth of strake vortices has a great influence in the body vortex, especially when the strake vortex is unsteady (greater

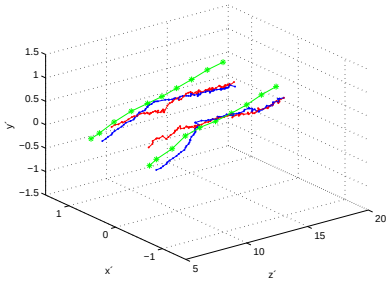

(a) 11°

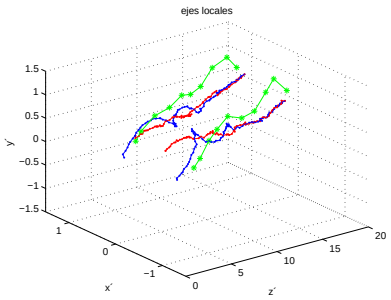

(b) 16°

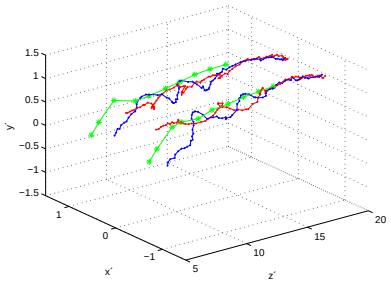

(c) 22°

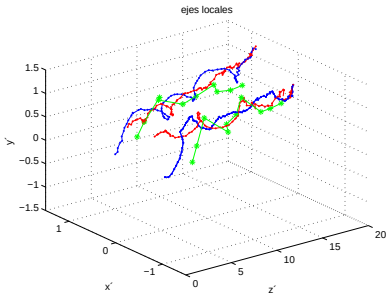

(d) 27°

FIGURE 17. NUMERICAL THREE DIMENSIONAL PATHS OF THE VORTEX CORES FOR 11°(a), 16°(b), 22°(c) and 27°(d)

than 20°). For these cases, the comparison between a slender body without strakes and the body-strake configuration has a key point related to the vortex position of the core. Thus, the average position of the vortex core is located at larger distances from the missile in comparison to the body without strakes. On the other hand, it is observed that the axial position at which the two vortices merge into one depends linearly on the angle of attack for the cases studied in this experimental work.

The numerical simulations show good correlation of the vortex positions with the experimental tests even though the speed regimes are significantly different. More significantly, the onset of strake vortex unsteadiness is the same for both the subsonic (experimental) and supersonic (numerical) simulations. Unfortunately the numerical simulations do not display the dynamic convective interaction between the body vortex and strake vortex sheet, though the positions correlate reasonably well with the average of the body and strake vortices. Further investigation into these discrepancies are recommended.

ACKNOWLEDGMENT

This work has been supported by Grant Proyecto de Excelencia de la Junta de Andalucia number P08-TEP-3867.

REFERENCES

[1] Nielsen, J., 1988. *Missile Aerodynamics*. Nielsen Engineering and Research, Inc.

[2] Moore, F., 2000. *Approximate Methods for Weapon Aerodynamics*. (American Institute of Aeronautics & Astronautics.

[3] Sigal, A., and Blake, W., 2007. "Aerodynamic analysis of body-strake configurations aiaa 2007-3939". pp. 659–678.

[4] Simpson, G., and Birch, T., 2001. "Some aerodynamic characteristics of missiles having very low aspect ratio wings". *AIAA 2001-2410*.

[5] Tuling, S., and Dala, L., 2010. "Some aspects of modelling very low aspect ratio wings in slender body configurations". *Royal Aeronautical Society Applied Aerodynamics Conference*, July.

[6] C. del Pino, L. Parras, M. F., and Fernandez-Feria, R., 2011. "PIV measurements of the structure of wing-tip trailing vortices and their comparison with theoretical models". *Physics of Fluids*(23), 013602.

[7] C. del Pino, J.M. Lopez-Alonso, L. P., and Fernandez-Feria, R., 2011. "Dynamics of the wing-tip vortex in the near field of a NACA 0012 aerofoil". *The Aeronautical Journal*(115), p. 1164.

[8] Jeong, J., and Hussain, F., 1995. "On the identification of a vortex". *J. Fluid Mech.,* ***285***, pp. 69–94.